

# Molecular dynamics simulation of liquid argon flow at platinum surfaces

J. L. Xu, Z. Q. Zhou

**Abstract** The micro Poiseuille flow for liquid argon flowing in a nanoscale channel formed by two solid walls was studied in the present paper. The solid wall material was selected as platinum, which has well established interaction potential. We consider the intermolecular force not only among the liquid argon molecules, but also between the liquid argon atoms and the solid wall particles, therefore three regions, i.e. the liquid argon computation domain, the top and bottom solid wall regions are included for the force interaction. The present MD (Molecular Dynamics) simulation was performed without any assumptions at the wall surface. The objective of the study is to find how the flow and the slip boundaries at the wall surface are affected by the applied gravity force, or the shear rate. The MD simulations are performed in a non-dimensional unit system, with the periodic boundary conditions applied except in the channel height direction. Once the steady state is reached, the macroscopic parameters are evaluated using the statistical mechanics approach. For all the cases tested numerically in the present paper, slip boundaries occur, and such slip velocity at the stationary wall surface increases with increasing the applied gravity force, or the shear rate. The slip length, which is defined as the distance that the liquid particles shall travel beyond the wall surfaces to reach the same velocity as the wall surface, sharply decreases at small shear rate, then slightly decreases with increasing the applied shear rate. We observe that the liquid viscosity remains nearly constant at small shear rates, and the Newtonian flow occurs. However, with increasing the shear rate, the viscosity increases and the non-Newtonian flow appears.

**Keywords** Molecular dynamics simulation, Poiseuille flow, Velocity profile, Slip length, Viscosity

## List of Symbols

$A$	slab area by $L_x L_y$ , $m^2$
$a$	acceleration, $m/s^2$
$F_{ij}$	intermolecular force between particle $i$ and $j$ , N
$g$	“gravity” acceleration, $m/s^2$
$H_n(z_i)$	function defined in Eq. (11)
$\vec{i}$	particle $i$
$\vec{i}$	unit vector in axial coordinate
$j$	particle $j$
$j_w$	solid particle $j_w$
$J_N$	parameter averaging starts at $J_N$ time step
$J_M$	parameter averaging stops at $J_M$ time step
$K_B$	Boltzaman constant, $1.38 \times 10^{-23}$ J/K
$L_x, L_y, L_z$	length of calculation domain in $x, y$ and $z$ coordinates, m
$L_s$	slip length of the fluid particle at the wall surface, m
$m$	mass of an argon atom, kg
$N$	total number of fluid particles in the calculation domain (box)
$N_{bottom}$	bottom solid wall molecule number
$N_{top}$	top solid wall molecule number
$N_w$	total number of solid particles of both up and bottom walls
$r$	vector coordinate from particle $i$ to particle $j$
$r_c$	cut-off distance between two fluid particles, m
$r_{cw}$	cut-off distance between fluid particles and solid wall particles, m
$T$	temperature, K
$T_w$	wall temperature, K
$T_{fluid}$	liquid temperature, K
$t$	time, s
$u$	average velocity, m/s
$u_w$	fluid velocity at the wall surface, m/s
$\phi$	potential, J
$v_x, v_y, v_z$	liquid velocity in $x, y$ and $z$ direction, m/s
$x, y, z$	coordinate in $x, y$ and $z$ direction
$\Delta z$	slab width in $z$ direction, m
$\rho$	liquid particle number density, $1/m^3$
$\rho_{wf}$	solid wall particle number density, $1/m^3$
$\varepsilon$	energy scale of the liquid particle, J
$\varepsilon_{wf}$	energy scale between fluid and solid particles, J
$\sigma$	length scale of the fluid particles, m
$\sigma_{wf}$	length scale between fluid and solid particles, m

Received: 3 January 2003  
 Published online: 28 October 2003  
 © Springer-Verlag 2003

J. L. Xu (✉), Z. Q. Zhou  
 Guangzhou Institute of Energy Conversion,  
 Chinese Academy of Sciences, No.81 Xianlie Zhong Rd.,  
 Guangzhou, 510070, P.R. China  
 E-mail: xujl@ms.giec.ac.cn  
 Tel.: +86-20-87624728  
 Fax: +86-20-87624728

The authors would like to thank for the financial support by the National Natural Science Foundation of China with the contract number of 10272102.

$\tau$	characteristic time of liquid particles, s
$\tau_w$	wall shear stress, Pa
$\mu$	fluid viscosity at the wall surface, kg/ms

## 1 Introduction

Consider the classical steady Poiseuille flow confined between two parallel wall surfaces from macroscale point of view. For developed flow between parallel plates the streamlines are parallel to the plates so that  $u = u(z)$  only and  $v = w = 0$ . We assume that the flow is only initiated by the gravity force and there is no additional applied force, or pressure gradient across the channels. For the present simple problem, the classical Navier-Stokes equation for the x-direction can be reduced as:

$$\mu \frac{\partial^2 u}{\partial z^2} + \rho g = 0 \quad (1)$$

Eq. (1) has the following solution satisfying the no-slip boundary conditions at the two wall surfaces positioned at  $z = 0$  and  $z = L$ :

$$u = \frac{\rho g}{2\mu} (Lz - z^2) \quad (2)$$

where  $L$  is the channel height in  $z$ -direction.

In recent years, due to the high demand of the information and biological technologies, flow and heat transfer in nano and micro scale attracted many scientists and engineers. Up to now there are a lot of articles dealing with gas flow in microchannels. Knudsen number which is defined as the gas mean free path divided by the channel dimension, is used to characterize the gas flow in microchannels. The Knudsen number regimes were developed by Gad-el-Hak [1] to decide which model should be used to compute the gas flow in a micro device. Readers who are interested in the gas flow in microchannels may read the recent review paper by Rostami, Mujumdar and Saniei [2].

However, there is little numerical/analytical work for liquid flow in microchannels in nano and micro scales. Some of the work in this field involves the experimental measurement. Due to the high difficulties in instrumentation, such measurements sometimes results in the larger uncertainties. Examination of the literature on liquid flow in microchannels leads to contradictory conclusions. In review of the related articles we shall use the concepts of apparent viscosity,  $\mu_a$  and the bulk value of the viscosity  $\mu_b$  at large distances from the wall surface. The apparent viscosity  $\mu_a$  is not a material property but a characteristic of the flow field. Different from the classical continuum mechanics in macroscale, the flow field in microchannels depends on the liquid type, the channel size and the surface material properties. Israelachvili [3, 4] has done a consideration work concerning viscous work in thin films. They demonstrated that for films thicker than ten molecular layers or 5 nm,  $\mu_a$  was about the same as  $\mu_b$ . For thinner films,  $\mu_a$  depends on the number of molecular layers and can be as high as  $10^5$  times larger than  $\mu_b$ . Chan and Horn [5] reported that  $\mu_a$  shows no much differences in films as thinner as 50nm and it increases in thinner

films. The experiment facilities used by Israelachvili, and Chan and Horn consists of two crossed cylinders with a small gap in between. The flow in their apparatus is considerably different from the Poiseuille flow in capillaries. Other researchers studied liquid flow in small capillaries and found that  $\mu_a$  and  $\mu_b$  were approximately equal. In contrast, Debye and Cleland [6] reported  $\mu_a$  smaller than  $\mu_b$  for paraffin flow in porous glass with average pore size several times larger than molecular size.

The above mentioned work involved the experimental measurements of the pressure drop and the flow rate across the flow channels. Recently Maynes and Webb [7] performed the detailed velocity profile measurements in a capillary tube with inside diameter of 705  $\mu\text{m}$  using micro molecular tagging velocimetry ( $\mu\text{MTV}$ ) at different flow rates. Because the tube diameter they used is relatively larger, the "microscale" effect may not occur. Thus the slip boundary has not been observed. To author's knowledge, there is no direct measurements of the slip boundary for the liquid flow in nano and micro scales. This is partially due to the high difficulties for the instrumentation. Flows in microscale devices differ from their macroscale characteristics for two reasons: the small scale makes molecular effects such as wall slip more important, and it amplifies the magnitudes of certain ordinary continuum effects to extreme levels. Fluid that are Newtonian at ordinary shear rate can become non-Newtonian at extremely high shear rate. The pressure gradient becomes very large in small cross section channels.

Electrokinetic effects take place at the wall surface such as glass due to chemical interaction, which induces an electrically charged double layer that results in a very thin layer of liquid close to the wall. Applying an electric field to this layer creates a body force capable of moving the liquid as if it were slipping over the wall.

Liquids have the densities which are about one thousand times of the gases. Molecules are packed with each other more closely. Molecular effects are difficult to compute in liquids because the transport theory is less well established than the kinetic theory for the gases. In dilute gases, intermolecular forces have little effect on the transport process. The molecules spend most of times in free flight between the collisions. The random molecular motions are responsible for the gaseous transport process. However, liquids are closely packed with each other and they are always in a collision state. When we apply a shear force, a velocity gradient must be created so that molecules will move relative to one another. On the average, the sum of all intermolecular forces must balance the imposed shear (Gad-el-Hak, [1]).

MD simulation ensures one go directly to the molecular level to see "what happen in small size channels". Koppik et al [8] performed the MD simulation to investigate the microscopic aspects of several slow viscous flows past a solid wall. They observed that systems including several thousand molecules can have reasonable continuum behavior. In Couette and Poiseuille flow, the no-slip boundary conditions occur naturally as a consequence of molecular roughness, the velocity profiles agree with the solutions of the Navier-Stokes equations. The slip boundary condition appears at lower densities. The above

conclusion can only be correct if one neglects the solid-liquid interactions. The investigation of the homogeneous-shear nonequilibrium molecular dynamics for a simpler solid-liquid interaction was carried out by Liem et al [9]. Three regions: the top solid wall region, the fluid molecule region, and the bottom solid wall region, were included in the calculation domain. For simplicity, the particles in the wall boundaries are exactly the same as those in the fluid, the same potential acts among all the particles including the wall layers. The boundary particles, however, are subjected to an additional harmonic potential. Because the solid wall particles were treated just as the fluid molecules, the calculation results lead to no-slip solution. Liquid flow in microchannels depends on the fluid molecules themselves, the wall material, and the coupling parameters such as length scale and energy scale between the fluid molecules and the wall particles. Assuming the simple liquid argon, whose potential is well established, is moving past the solid wall surface, the slip at the surface depends on the force interactions among the argon molecules, and between the argon molecules and solid wall molecules. MD simulations of Lennard-Jones liquids sheared by two solid walls were performed by Thompson and Robbins [10]. Slip was found to be directly related to the amount of structure induced in the fluid by the periodic potential from the walls. Slip occurred when there is a weak interaction between the fluid and the solid wall molecules. Later Thompson and Troian [11] performed the MD simulation of the Couette flow for the unit cell measured  $12.51\sigma \times 7.22\sigma \times h$  where  $h$  varied from  $16.71\sigma$  to  $24.57\sigma$  corresponding to about one thousand fluid molecules. The velocity profiles in nondimensional unit was plotted against the nondimensional length for different wall-fluid coupling parameters. Both slip and no-slip phenomena were observed.

In the present paper, we computed the liquid argon flow confined between two parallel wall surfaces. The flow is initiated by applying a uniform gravity force for each liquid molecules. The wall is stationary and the surface material is chosen to be platinum. Applying MD simulation approach, we obtained the steady liquid particle number density, mean velocity, temperatures etc across the two wall surfaces. More attention was paid to the phenomenon at the wall surface, including the slip length and the liquid viscosities.

## 2

### Calculation domain and MD simulation approach

In the present paper, three regions were included in the model: the top solid wall, the liquid argon and the bottom solid wall regions. The liquid calculation domain, with three lengths of  $L_x$ ,  $L_y$  and  $L_z$ , is illustrated in Fig. 1 for 1372 argon molecules in the liquid calculation domain, and 1600 solid molecules of top and bottom wall regions. The other two run cases involve 256 argon molecules, 576 solid molecules, and 864 argon molecules, 1296 solid molecules, respectively. The materials of both top and bottom solid walls are platinum, the molecules are arranged in face-centered-cubic (fcc) structures. Because the MD simulation can only treat a limited number of molecules, the computed lengths for both top and bottom

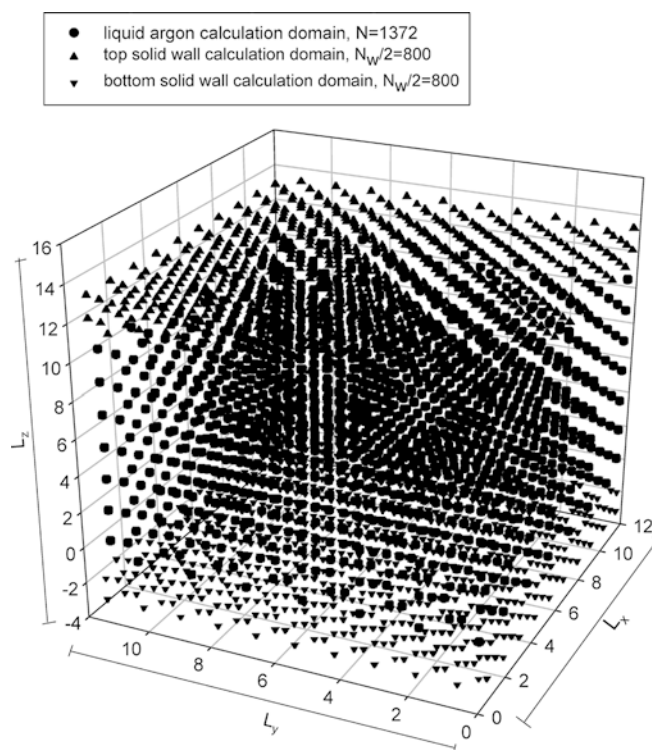


Fig. 1. Calculation domain for liquid argon, top and bottom solid wall regions

walls in  $x$  and  $y$ -directions are necessary to be specified. Physically the two infinity walls in  $x$  and  $y$ -directions are considered by the periodic boundary condition approach. The top and bottom walls include several molecular layers in  $z$ -direction such that the distance between any liquid argon molecule and the solid wall molecules beyond the selected solid wall layers are out of the cut-off range. The reason of choosing wall particles as platinum and liquid molecules as argon is that these molecules have well-established molecular potential interaction. Because we deal with the Poiseuille flow confined between two solid walls, all the wall particles are assumed to be stationary. The total number of both top and bottom wall particles is  $N_w$ , the number of liquid argon in the liquid calculation domain is  $N$ . The distance between adjacent solid molecules is  $2.77 \times 10^{-10}$  m and the spring force constant is 46.8 N/m (Maruyama and Kimura [12]). Any argon molecule in the calculation domain has the force interaction with not only its neighboring argon molecules in the liquid calculation domain, but also with the top and bottom solid wall molecules. In addition to these, the argon molecules have the applied gravity force, as if they were falling under gravity force. By varying the applied gravity force, the corresponding shear rate at the wall surface can be changed.

The MD simulations start from the integration of the Newton's second law. Applying the Gear finite-difference algorithm, the basic dynamic parameters such as position, velocity and interaction force can be determined. The macroscopic physical properties such as pressure, mean velocity, temperature, particle number density can subsequently be calculated via statistical mechanics. Based on

this idea, the Newtonian equations for each liquid molecule is written as

$$m_i \frac{d\vec{r}^2}{dt^2} = \sum_{j \neq i, j=1}^N \vec{F}_{ij} + \sum_{j_w \neq i, j=1}^{N_w} \vec{F}_{ij_w} + m_i g \vec{i} \quad (3)$$

where subscript  $i$  represents particle  $i$ ,  $\vec{i}$  is the unit vector in x-coordinate. The first term of right hand side of Eq. (3) is the molecular force due to Lennard-Jones potential between particle  $i$  and other liquid molecules in the liquid calculation domain, the second term is the molecular force between particle  $i$  and all the solid wall particle  $j$ . It is clear that the third term represents the applied gravity force specified in x-direction. When a two-body potential model is applied, the interaction force between a pair of molecules is given by the following relation:

$$F_{ij} = -\frac{\partial \phi_{ij}}{\partial r_{ij}} \quad (4)$$

The Lennard-Jones potential  $\phi_{ij}$  is written as:

$$\phi(r) = 4\epsilon \left[ \left( \frac{\sigma}{r} \right)^{12} - \left( \frac{\sigma}{r} \right)^6 \right] \quad (5)$$

where  $\sigma = 3.4 \times 10^{-10}$  m and  $\epsilon = 1.67 \times 10^{-21}$  J, they are length and energy scale of liquid argon molecules. The cut-off distance is set to be  $2.5\sigma$ . The interaction between liquid argon particles and the platinum molecules also follow the same expression as Eq. (5), but the values of the  $\sigma$  and  $\epsilon$  parameters are changed to be  $3.085 \times 10^{-10}$  m and  $0.894 \times 10^{-21}$  J, respectively, as suggested by Poulikakos and Yadigaroglu [12]. They are named as  $\sigma_{wf}$  and  $\epsilon_{wf}$ . Note that when Eq. (5) is applied for the potential interaction between liquid particles and solid wall particles, the cut-off length is changed to be  $2.5 \sigma_{wf}$  correspondingly.

Finally combining Eq. (4),(5) into Eq. (3) and applying the shifted potential and shifted force concepts as described by Haile [13], we obtain the basic equation for each liquid argon particle. The shifted force technique ensures that the molecular force between liquid particle  $i$  and other liquid particles or other solid wall particles is reduced to zero once the distance between these particles reaches or is beyond the cut-off distance. The main advantage of doing this is to save a lot of computation time for the force integration.

$$\begin{aligned} 24 \frac{\epsilon}{\sigma} \sum_{j \neq i, j=1}^N \left[ 2 \left( \frac{\sigma}{r} \right)^{13} - \left( \frac{\sigma}{r} \right)^7 - 2 \left( \frac{\sigma}{r_c} \right)^{13} + \left( \frac{\sigma}{r_c} \right)^7 \right] \frac{\vec{r}_{ij}}{|r_{ij}|} \\ + 24 \frac{\epsilon_{wf}}{\sigma_{wf}} \sum_{j_w=1}^{N_w} \left[ 2 \left( \frac{\sigma_{wf}}{r} \right)^{13} - \left( \frac{\sigma_{wf}}{r} \right)^7 - 2 \left( \frac{\sigma_{wf}}{r_{cw}} \right)^{13} + \left( \frac{\sigma_{wf}}{r_{cw}} \right)^7 \right] \\ \times \frac{\vec{r}_{ij_w}}{|r_{ij_w}|} + m_i g \vec{i} = m_i \vec{a}_i \quad (6) \end{aligned}$$

## 2.1 Thermal wall model

The present model involves the real potential and force interaction between the liquid argon particles and the two

solid wall particles without any assumptions. Considering the situation that a liquid argon particle is quite close to the wall surface, the repulsive force between the liquid particles and the solid molecules will push the liquid particle away from the wall surfaces. Theoretically such force interaction will never let the liquid particles penetrate the wall surfaces. However, in the real computation, we can not guarantee that no liquid particles travel beyond the wall surfaces. This is because it is impossible to use an infinity small time step. Due to the above reason, we incorporate the thermal wall model into the present work as an accessorial boundary conditions. By monitoring the computation process through the time series, for most time steps, there is no particle beyond the wall surface. Accidentally, there are some time steps that have a couple of particles striking the wall surfaces. Under that situation, we incorporate the thermal wall model to ensure that all the liquid particles confined in the two parallel walls.

In the previous studies, MD simulations were applied to various types of boundaries (for example, specular surfaces, periodic boundaries, and thermal walls). In the present report, the thermal wall models are employed. When a liquid particle strikes a thermal wall at temperature  $T_w$ , all three components of velocities are reset to a biased Maxwellian distribution. The three velocity components after the liquid particles striking the wall surfaces are (Alexander and Garcia [14]):

$$\begin{aligned} v_x &= \sqrt{\frac{k_B T_w}{m}} \psi_G, \\ v_y &= \sqrt{\frac{k_B T_w}{m}} \psi'_G, \\ v_z &= \pm \sqrt{-\frac{2k_B T_w}{m} \ln \psi} \end{aligned} \quad (7)$$

The positive sign of  $v_z$  is for the liquid particles striking the bottom wall surface, while the negative sign is for the liquid particles striking the top wall surface.  $\psi$  is an uniformly distributed random number in (0,1) and  $\psi_G, \psi'_G$  are Gaussian-distributed random numbers with zero mean and unit variance.

The detailed reentry mechanism at the thermal wall is described by Tenenbaum et al. [15]. As discussed already, using other types of boundaries has no obvious influence on the macroscopic parameters. In other words, our calculation results show that the present model is insensitive to the selected accessorial wall models. The macroscopic parameters are mainly governed by the liquid-solid molecular interaction.

Because both of top and bottom walls are not moving, the velocities of wall particles are set to be zero. The particles are fixed in the specified positions in the face-centered-cubic (fcc) structure.

## 2.2 Initial conditions

The initial conditions include the information of the two solid walls and the liquid argon regions to initiate the numerical computation. The procedure is summarized as follows:

- The solid wall molecules are arranged in fcc structure and such arrangement is not changing during the whole

calculation process, because the two solid walls are stationary.

- The initial positions of liquid argon molecules are structured in fcc. However, the liquid molecules will deviate from the initial positions once the applied gravity force acts on the liquid molecules.
- A random distributed velocities in the liquid argon region are assumed to initiate the calculation. However, in order to make sure that the steady state can be easily reached after some reasonable time running, the random distributed velocities should satisfy that the total kinetic temperature is equal to the kinetic energy in the liquid calculation domain:

$$\frac{3}{2}Nk_B T_{fluid} = \frac{1}{2}m \sum_{i=1}^N (v_{i,x}^2 + v_{i,y}^2 + v_{i,z}^2) \quad (8)$$

- Values for the initial acceleration  $a_i(0)$  are determined in terms of the positions  $r_i(0)$  by computing the force on each atom, using the Newtonian's second law. The Gear finite-difference algorithm also needs the higher derivatives. These higher time derivatives are assumed to be zero for the initial time step to initiate the calculation.

$$\begin{aligned} x_i'''(0) &= x_i^{iv}(0) = x_i^v(0) = 0 \\ y_i'''(0) &= y_i^{iv}(0) = y_i^v(0) = 0 \\ z_i'''(0) &= z_i^{iv}(0) = z_i^v(0) = 0 \end{aligned} \quad (9)$$

## 2.3

### Periodic boundary conditions

Because we can only calculate a limited particle numbers of liquid and wall, the two infinity walls are represented by the specific lengths in x and y-directions combing with the periodic boundary conditions in these two coordinates. The final calculation results such as the velocity distributions across the z-direction, the slip length, etc are not influenced by the selected computation length in x and y-direction. When a liquid particle is leaving the boundary at  $x = 0$  or  $x = L_x$ , a corresponding liquid particle will enter the liquid argon calculation domain at  $x = L_x$  or  $x = 0$ . The particle entering the calculation domain has the same velocities as the liquid particle that is leaving the calculation domain.

Similarly, particles leaving the liquid argon calculation domain at  $y = 0$  or  $y = L_y$  have the corresponding particles that enter the argon domain. This principle ensures that the total liquid molecule number in the calculation domain is constant.

When we perform the molecular force interaction, the image force shall be included. For instance, liquid particle  $i$  has the molecular interaction with particle  $j$  in the liquid calculation domain. However, particle  $j$  located at  $(x_j, y_j, z_j)$  has a series of image particles outside of the calculation domain located at  $(x_j \pm nL_x, y_j \pm mL_y, L_z)$  where  $n$  and  $m$  are integers ranging from 1 to infinity. In order to reduce the computation time for the force calculation of particle  $i$  with any particle  $j$  in the liquid calculation domain and its particle images, Eq. (4) is corrected in terms of Haile [13]:

$$\vec{F}_{ij} = - \sum_{\alpha_x=-1}^{\alpha_x=1} \sum_{\alpha_y=-1}^{\alpha_y=1} \frac{d\phi_{ij}(\vec{x}_{ij} - \alpha_x \vec{L}_x, \vec{y}_{ij} - \alpha_y \vec{L}_y, \vec{z}_{ij} - \alpha_z \vec{L}_z)}{d\vec{r}_{ij}} \quad (10)$$

Eq. (10) accumulates forces for molecule  $i$  interacted with atom  $j$  inside the liquid calculation domain and its images outside of the liquid argon calculation domain. Note that Eq. (10) is also valid for the force integration between particle  $i$  with any solid wall particle  $j_w$  and its images outside of the two solid wall regions.

A minimum-image criterion has been developed to perform the real sum of Eq. (4) and Eq. (10). For a cubic container in three dimensions, the minimum image criterion applies separately to each Cartesian component of the pair separation vector. For the  $x$  component, we use  $x_{ij} \rightarrow x_{ij} - \alpha_x L_x$  where  $\alpha_x = 0$  if  $-0.5L_x \leq x_{ij} \leq 0.5L_x$ ,  $\alpha_x = -1$  if  $x_{ij} \leq -0.5L_x$ , and  $\alpha_x = 1$  if  $x_{ij} \geq 0.5L_x$ , as suggested by Haile [13]. Similarly for  $y_{ij}$ . There is no image effect on the  $z$  component.

## 2.4

### Parameter averaging

The Gear finite-difference algorithm was performed for the dynamic simulation of the molecular system. The time step is chosen from  $\Delta t = 0.005\tau$  to  $\Delta t = 0.0005\tau$  depending on the amplitude of the applied force, where  $\tau$  is the Lennard-Jones nondimensional time  $\tau = \sigma\sqrt{m/\epsilon}$ . For large applied gravity force (large shear rate), the liquid particle has a small characteristic time response to the large applied gravity force. In order to match the small characteristic time resulted from the large gravity force with the molecular oscillation time  $\tau$ , we use a small time step. For instance, for the nondimensional gravity force of 5.0, a time step of  $\Delta t = 0.0005\tau$  is used. Smaller time step will not result in any change of the flow field. For most run cases, following the integrated time of  $100\tau$ , the system has evolved into the steady state. The liquid calculation domain is divided into many bins. The number of bins is dependent on the liquid molecule numbers. For larger liquid number system, more bins are divided. The macroscopic parameters, such as the number density, mean velocity, temperatures etc. are defined in the center of each bin. These parameters can be obtained via statistical mechanics, and the detailed procedures are summarized as follows. For the present problem, we calculate these parameters as a function of  $z$ . We define the function  $H_n(z_i)$  such that

$$H_n(z_{ij}) = 1 \quad \text{if } (n-1)\Delta z < z_i < n\Delta z, \quad (11)$$

otherwise,  $H_n(z_{ij}) = 0$ .

where the subscript  $j$  represents the  $j$  time step.

Then the average non-dimensional number density in  $n$ -th bin from  $J_N$  time step to  $J_M$  time step is

$$\rho_n \sigma^3 = \frac{\sigma^3}{A\Delta z(J_M - J_N + 1)} \sum_{j=J_N}^{J_M} \sum_{i=1}^N H_n(z_{ij}) \quad (12)$$

where  $z_i$  is the coordinate of the midpoint of the  $n$ -th bin,  $A$  is the area expressed as  $L_x \times L_y$ .  $J_N$  and  $J_M$  are the start

and ending time step of the parameter averaging. The integrated time interval from  $J_N$  time step to  $J_M$  time step is larger than  $150\tau$ . Longer time interval also results in no change of the parameter averaging. The bin average velocity from  $J_N$  time step to  $J_M$  time step is given by:

$$u(z_i) = \frac{1}{(J_M - J_N + 1) \sum_{i=1}^N H_n(z_{ij})} \sum_{j=J_N}^{J_M} \sum_{i=1}^N H_n(z_{ij}) v_{ij}^x \quad (13)$$

where  $v_{ij}^x$  is the velocity in  $x$  component of particle  $i$  at  $j$  time step. Using Eq. (13), we compute the bin temperature as

$$T(z_i) = \frac{1}{3k_B(J_M - J_N + 1) \sum_{i=1}^N H_n(z_{ij})} \times \sum_{j=J_N}^{J_M} \sum_{i=1}^N H_n(z_{ij}) m_i [v_{ij}^x - u^x(z_i)]^2 \quad (14)$$

where the superscript  $\alpha$  represents  $x, y$ , or  $z$ . At steady state,  $u^y(z_i)$  and  $u^z(z_i)$  are zero for all the bins.

Considering the liquid argon calculation domain with the volume of  $L_x \times L_y \times L_z$ , once the steady state is reached, the ‘‘gravity’’ force of the  $N$  liquid particles should be balanced by the wall friction force of the top and bottom solid walls, we have:

$$Nmg = 2\tau_w L_x L_y \quad (15)$$

where the left hand side of Eq. (15) is the total particle gravity force and the right hand side of Eq. (15) is the friction force.  $\tau_w$  is the shear stress. The liquid viscosity at the wall surface is defined as ‘‘the shear stress divided by the velocity gradient at the wall surface’’.

$$\mu = \frac{\tau_w}{\left. \frac{du(z)}{dz} \right|_w} \quad (16)$$

where  $\left. \frac{du(z)}{dz} \right|_w$  is the velocity gradient (we also name it as shear rate) at the wall surface.

In the previous MD simulation (Kopiik et al. [8], Liem et al. [9]), shear stress involves the particle force integration. The viscosity in terms of this approach sometimes gets a higher uncertainty. The present paper provides a better and easy way which has a clear physical meaning to obtain the wall shear stress and viscosity using Eqs. (15) and (16) with high accuracies than the previous study.

One of the major differences between the liquid flow in nano and micro scale and the classical fluid mechanics is that the liquid flow in small size have the slip boundary condition. Such slip boundary condition can be obtained from the computed mean velocity profile. The slip length shows how much degree that the flow deviates from the classical fluid mechanics with no-slip boundary condition, and is defined as ‘‘how far the fluid should travel beyond the solid wall to reach the same velocity as the wall surface’’. The slip length is calculated as

$$L_s = \left| \frac{u_w}{\left. \frac{du(z)}{dz} \right|_w} \right| \quad (17)$$

## 3 Results and discussion

### 3.1 Nondimensional unit system

We developed a code named as ‘‘MDARGON’’ using the nondimensional system. Note that Eq. (6) is written in unit system. Using the following parameters in nondimensional units,

$$\begin{aligned} r^* &= \frac{r}{\sigma}, & x^* &= \frac{x}{\sigma}, & y^* &= \frac{y}{\sigma}, & z^* &= \frac{z}{\sigma} \\ t^* &= \frac{t}{\tau} \\ F^* &= \frac{F\sigma}{\varepsilon} \end{aligned} \quad (18)$$

$$v^* = v\sqrt{m/\varepsilon}$$

$$a^* = \frac{a}{\sigma/\tau^2} = \frac{\tau^2}{\sigma} a$$

Eq. (6) can be rewritten as

$$\begin{aligned} \bar{a}_i^* &= 24 \sum_{j \neq i, j=1}^N \left( \frac{2}{|r_{ij}^*|^{13}} - \frac{1}{|r_{ij}^*|^7} - \frac{2}{(r_c^*)^{13}} + \frac{2}{(r_c^*)^7} \right) \\ &\times \frac{(\vec{r}_i^* - \vec{r}_j^*)}{|r_{ij}^*|} + 24 \frac{\varepsilon_{wf}/\varepsilon}{\sigma_{wf}/\sigma} \\ &\times \sum_{j_w=1}^{N_w} \left[ \left( \frac{\sigma_{wf}}{\sigma} \right)^{13} \frac{2}{|r_{ij_w}^*|^{13}} - \left( \frac{\sigma_{wf}}{\sigma} \right)^7 \frac{1}{|r_{ij_w}^*|^7} - \frac{2}{|r_{c_w}^*|^{13}} + \frac{1}{|r_{c_w}^*|^7} \right] \\ &\times \frac{(\vec{r}_i^* - \vec{r}_{j_w}^*)}{|r_{ij_w}^*|} + \frac{m_i \sigma}{\varepsilon} \vec{g}_i \end{aligned} \quad (19)$$

The micro Poiseuille flow is governed by the parameters of liquid particle number  $N$ , density ratio of solid wall to liquid  $\rho_{wfl}/\rho$ , length scale ratio of solid wall to liquid  $\sigma_{wfl}/\sigma$ , energy scale ratio of solid wall to liquid  $\varepsilon_{wfl}/\varepsilon$ , and the applied nondimensional gravity force of  $\frac{m\sigma}{\varepsilon} g$ . For the liquid argon molecules interacted with the platinum solid molecules,  $\rho_{wfl}/\rho = 3.227$ ,  $\sigma_{wfl}/\sigma = 0.9074$  and  $\varepsilon_{wfl}/\varepsilon = 0.5353$ . Combing Eq. (15) and (16), we obtain the nondimensional viscosity as

$$\mu^* = \frac{\mu}{\varepsilon\tau\sigma^{-3}} = \frac{\rho\sigma^3 L_z^* m\sigma g}{2 \left. \frac{du}{dz} \right|_w^* \varepsilon} \quad (20)$$

Note that  $\rho\sigma^3$  is the liquid nondimensional number density and is 0.81 for the liquid argon.  $L_z^*$  and  $\left. \frac{du}{dz} \right|_w^*$  are the nondimensional channel length in  $z$  direction and the nondimensional velocity gradient at the wall surface.

The nondimensional slip length is coming from Eq. (17), and is rewritten as

$$L_s^* = \frac{L_s}{\sigma} = \frac{u_w^*}{\left. \frac{du}{dz} \right|_w} \quad (21)$$

### 3.2

#### Flow behavior dependent on the gravity force

The MD simulation was performed over a wide range of parameters including the calculation domains with three different particle numbers, and the applied nondimensional gravity force. The liquid is argon with the known molecular mass of  $m = 6.67 \times 10^{-23}$  g, length scale of  $\sigma = 0.34$  nm and energy scale of  $\varepsilon = 1.67 \times 10^{-21}$  J. The characteristic time scale is  $\tau = 2.16 \times 10^{-12}$  s. The liquid calculation domain is set to be cubic with the same lengths of  $L_x$ ,  $L_y$  and  $L_z$ . Such arrangement results in the length of  $L_z = 11.92\sigma$  (4.05 nm) for 1372 liquid molecules,  $L_z = 10.217\sigma$  (3.473 nm) for 864 liquid molecules, and  $L_z = 6.812\sigma$  (2.316 nm) for 256 liquid molecules, respectively. With varying the nondimensional gravity force, the flow shows three distinct characteristics, and they are described as follows:

At very small nondimensional gravity force, for most cases less than 0.05, the gravity force has no contribution to the mean axial velocity. The liquid molecules oscillate randomly in three coordinates due to the intermolecular force with zero mean velocities. The system is likely to be isolated without any applied force, or the pressure gradient. The flow is identified as “free molecular oscillation”. The typical velocity profile across the two wall surfaces is shown in Fig. 2 for the liquid argon number of 1372 and the nondimensional gravity force of 0.02. It is seen that the velocity is indeed zero across the two wall surfaces. The phenomenon is caused by the very small ratio of the gravity force to the intermolecular force. Under such conditions, the gravity force is so small that it can not establish the flow field across the two wall surfaces.

The coupling region appears when the nondimensional gravity force is increased. The flow is governed by not only the applied gravity force, but also the intermolecular force due to LJ potential. The flow oscillates in y and z direction

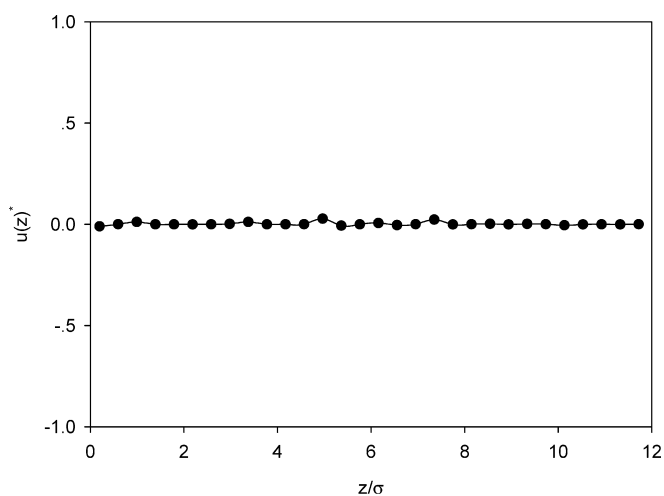


Fig. 2. Velocity profile across the two wall surfaces in the molecular free oscillation region ( $N = 1372$ ,  $N_{top} = N_{bottom} = 800$ ,  $m\sigma g/\varepsilon = 0.02$ )

with zero mean velocities, but the mean axial velocity can be established in x-direction. The slip boundary occurs at the wall surface, which is different from the classical Poiseuille flow in macroscales. The region is named as the “coupling region”. The flow behavior in the coupling region is most important in the present paper and is discussed in the following section separately.

Further increasing the nondimensional gravity force, the intermolecular force has no contribution to the mean axial velocity in x-direction. The flow has a uniform mean velocity profile across the two walls, but has a linear increase with time at a constant acceleration of the nondimensional gravity force. The nondimensional mean axial velocity can be expressed as  $u(z)^* = \frac{m\sigma g t}{\varepsilon \tau}$ . We refer this region as the “gravity force domain region”. The flat velocity profile across the two wall surfaces and the linear increase versus time are shown in Fig. 3 for the liquid argon number of 1372 and the nondimensional gravity force of 5.0. Such flat velocity distribution is caused by the high ratio of the gravity force to the intermolecular force such that each liquid molecule is falling under the high gravity force independently without the effect of the intermolecular force. Therefore each liquid molecule has the same velocity as others, leading to the even velocity profile across the two wall surfaces, but has a linear increase versus time. The transitions among the three regions are shown in Table 1.

### 3.3

#### Flow behavior in the coupling region

A typical run case for 1372 liquid molecules, 800 solid wall molecules for each solid wall regions at the nondimensional gravity force of 1.0 is shown in Fig. 4 for the liquid molecular distribution, and in Fig. 5 for the nondimensional number density and mean axial velocity distribution across the two solid walls when the steady state is fully reached. The corresponding nondimensional shear rate (velocity gradient) at the wall surface is 1.397, the nondimensional slip velocity at the wall surface  $u_w^*$  is 1.545 and

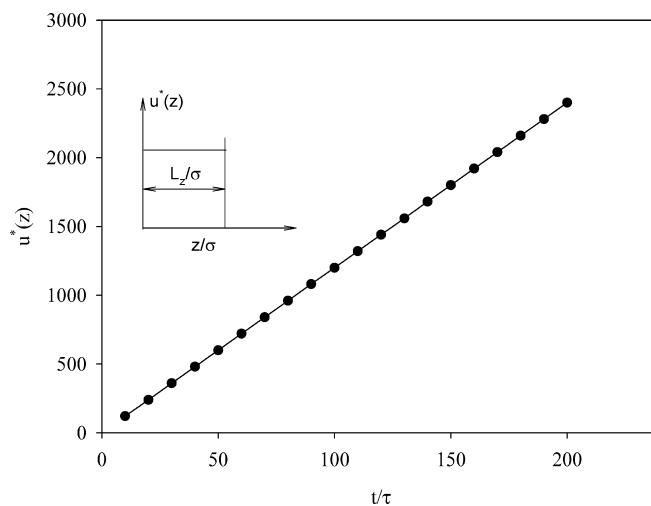
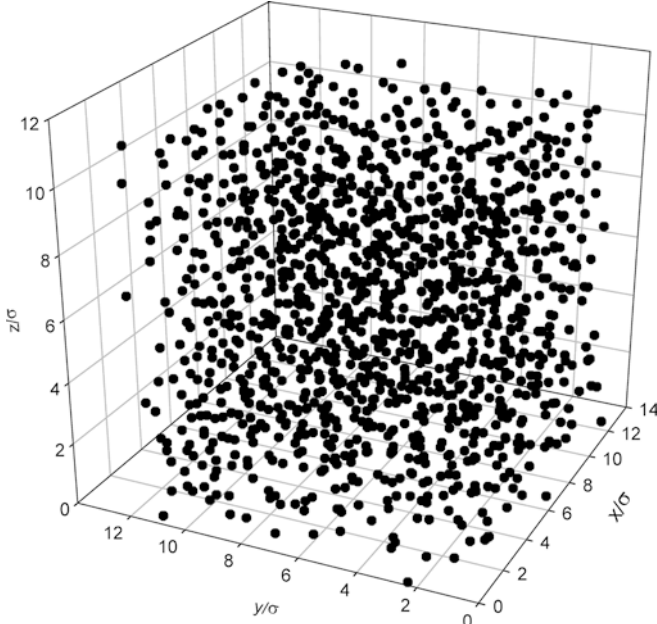


Fig. 3. Velocity profile across the two wall surfaces and velocity versus time in the gravity force domain region ( $N = 1372$ ,  $N_{top} = N_{bottom} = 800$ ,  $m\sigma g/\varepsilon = 5$ )

**Table 1.** Transitions among the three different regions

Run case	Fluid molecules	Top solid wall molecules	Bottom solid wall molecules	Free oscillation region	Coupling region	Gravity force domain region
1	256	288	288	$\frac{m\sigma g}{\varepsilon} < 0.05$	$0.05 \leq \frac{m\sigma g}{\varepsilon} \leq 3$	$\frac{m\sigma g}{\varepsilon} > 3$
2	864	648	648	$\frac{m\sigma g}{\varepsilon} < 0.05$	$0.05 \leq \frac{m\sigma g}{\varepsilon} \leq 2.5$	$\frac{m\sigma g}{\varepsilon} > 2.5$
3	1372	800	800	$\frac{m\sigma g}{\varepsilon} < 0.05$	$0.05 \leq \frac{m\sigma g}{\varepsilon} \leq 2$	$\frac{m\sigma g}{\varepsilon} > 2$



**Fig. 4.** Liquid argon distribution in the calculation domain at  $t = 150\tau$  ( $N = 1372$ ,  $N_{top} = N_{bottom} = 800$ ,  $m\sigma g/\varepsilon = 1.0$ )

the slip length  $L_s$  is  $1.106\sigma$ . The nondimensional viscosity  $\mu^*$  is 3.456, which is higher than the normal value of 2.0 at lower shear rate. Such flow behavior will be discussed later in detail. It is shown from Fig. 4 that the liquid molecules in the argon calculation domain has deviated from the initial fcc structure. The nondimensional number density shown in Fig. 5a has a uniform distribution in the channels, except that there are large oscillations near the two solid walls. Even though the oscillated number density distribution detected near the wall surfaces, the number density has a symmetric distribution about the centerline of the two solid walls located at  $z^* = L^*_z/2$ . The oscillation distribution of the molecular number density near the wall surfaces is caused by the strong solid-liquid intermolecular force interaction due to the LJ potential. However, away from the near wall region, the solid-liquid intermolecular force interaction will be in the cut-off range due to the short range interaction behavior, leading to the very small influence on the liquid number distribution thus a flat liquid number density distribution away from the near wall regions. As shown in Fig. 5b, the mean axial velocity profile across the two walls is also symmetric about the centerline of the two walls. The maximum mean axial velocity occurs at the centerline located at  $z^* = L^*_z/2$ . It is clear to identify the slip boundaries at the two wall surfaces, which is distinct from the classical Poiseuille flow in macroscale. The profile can be well correlated as a quadratic function as:

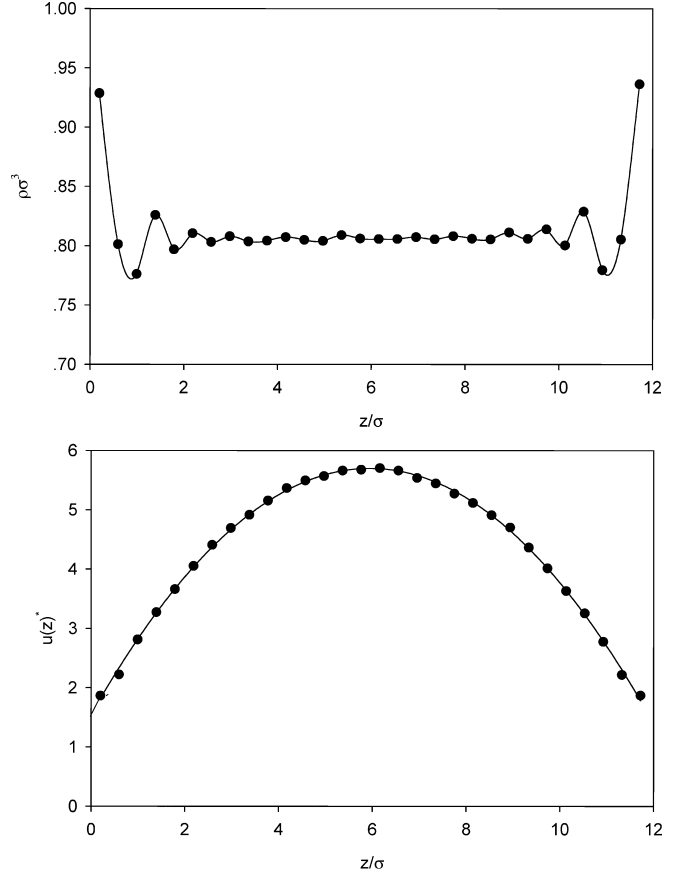


**Fig. 5.** The non-dimensional number density and velocity profile across the two solid walls ( $N = 1372$ ,  $N_{top} = N_{bottom} = 800$ ,  $m\sigma g/\varepsilon = 1.0$ )

$$u^*(z^*) = a_0 + a_1 z^* + a_2 z^{*2} \quad (22)$$

The coefficients of  $a_0$ ,  $a_1$  and  $a_2$  are based on the curve fitting of the velocity profile. Where  $a_0$  is the nondimensional slip velocity at the wall surface,  $u^*_w$ , while  $a_1$  is the nondimensional shear rate at the wall surface (or the nondimensional velocity gradient at the wall surface),  $(du/dz)^*_w$ . Once one obtains the coefficients of  $a_0$  and  $a_1$ , the nondimensional viscosity and the slip length at the wall surface can be easily computed in terms of Eqs. (20) and (21).

The effect of the nondimensional gravity force on the velocity profile is demonstrated in Fig. 6 for 864 liquid argon molecules, 648 solid wall molecules for each solid wall. It is shown that with increasing the nondimensional gravity force, the velocity profile has a higher distribution, while the slip velocity at the solid-liquid interfaces is also increased. Higher nondimensional gravity force will result in more uneven velocity profile distribution in the chan-



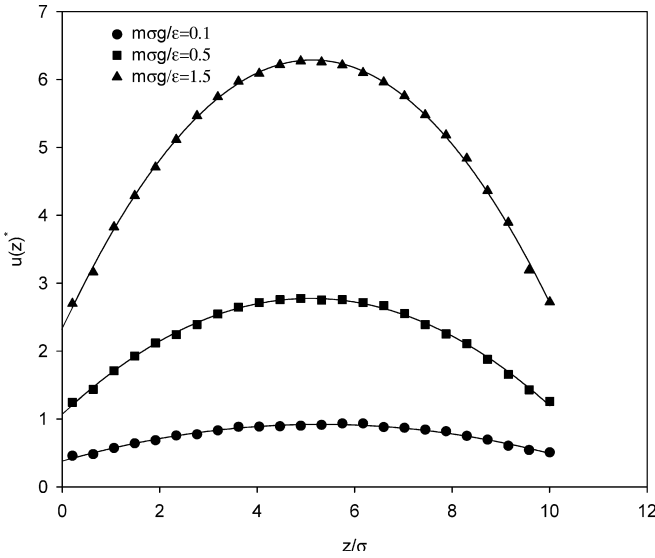


Fig. 6. Effect of gravity force on the mean axial velocity profile ( $N = 864, N_{top} = N_{bottom} = 648$ )

nels. It is easy understood that a higher nondimensional gravity force results in a higher mean velocity in the channel. Because the increase of the slip velocity at the wall surface can not match the increase of the mean velocity in the channel, the more uneven velocity profile is obtained with increasing the nondimensional gravity force.

A similar velocity profiles depended on the nondimensional gravity force and the liquid argon molecule numbers are shown in Fig. 7. At the same nondimensional gravity force, larger liquid argon system (larger size in channel height) will produce higher velocity profile.

### 3.4

#### Surface phenomenon

It is well known that the micro channels have a higher surface to volume ratio, making it more attractive for the electric cooling applications. In fact we deal with the surface characteristics in the present paper using the MD simulation, considering the intermolecular interactions between the liquid and solid molecules without any assumptions. The micro Poiseuille flow in nanoscale is well established by applying the gravity force for each liquid molecules. As illustrated in Fig. 8, the nondimensional shear rate at the wall surface is increased with increasing the nondimensional gravity force. Also shown in Fig. 8 is that the created shear rate is larger for larger liquid argon molecule system at the same gravity force.

In the present paper we use the slip velocities at the wall surface, the slip lengths and the viscosities to identify the surface characteristics. These results are presented versus the nondimensional shear rate at the wall surface in Fig. 9 and 10 for three different liquid argon molecule systems, respectively. The slip velocities at the wall surfaces is increased with increasing the wall shear rate, as described in Fig. 9. For most run cases, smaller liquid argon molecule system will get a higher slip velocities when the wall shear rate is fixed. Such trend is consistent with that a very large liquid argon system will have a zero slip velocities,

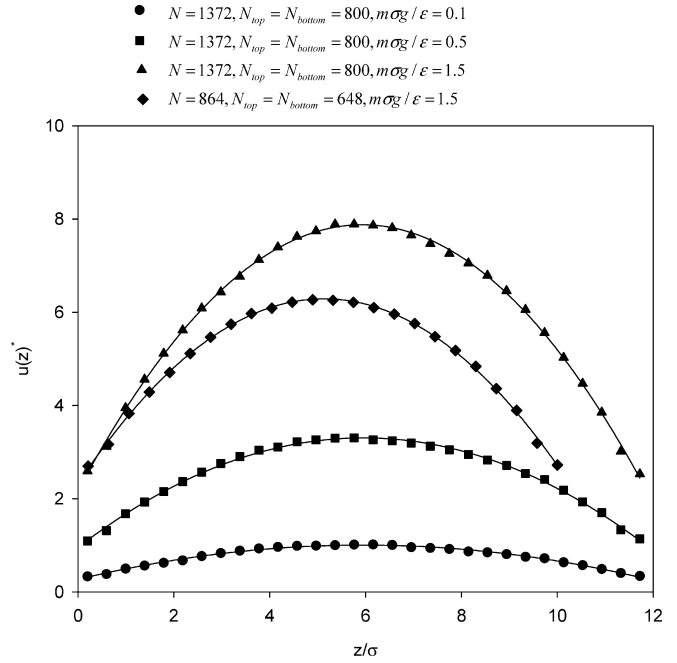


Fig. 7. Effect of gravity force and channel size on the mean axial velocity profile

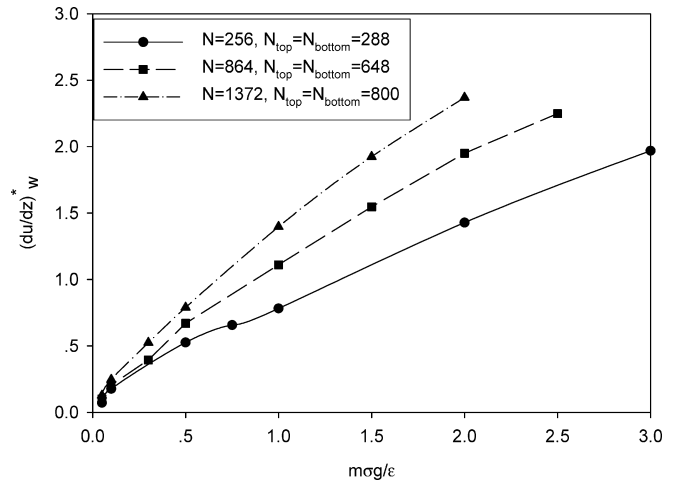


Fig. 8. The nondimensional shear rate versus the applied nondimensional gravity force

approaching to the classical Poiseuille flow solutions in macroscales.

The slip velocity is an important parameter to characterize the surface phenomenon in small sizes. Theoretically the slip velocity at the wall surface is caused by the strong solid-liquid intermolecular force interaction near the wall region. However, such intermolecular force is a short range interaction within two to three molecular layers. With increasing the channel height in  $z$ -direction due to the increased liquid number, the influence of the near wall solid-liquid interaction on the whole velocity profile across the two wall surfaces is decreased, leading to a smaller slip velocity when the wall shear rate is fixed. Further study is suggested for more liquid number system, but this is limited by the computer speed and memory because MD

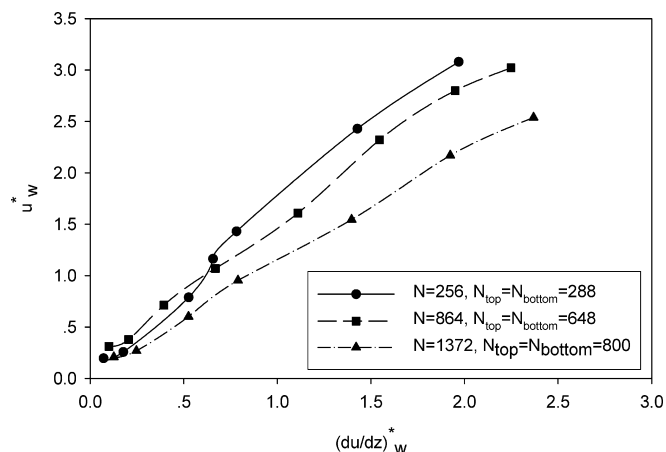


Fig. 9. Effect of shear rate on the slip velocity at the wall surfaces

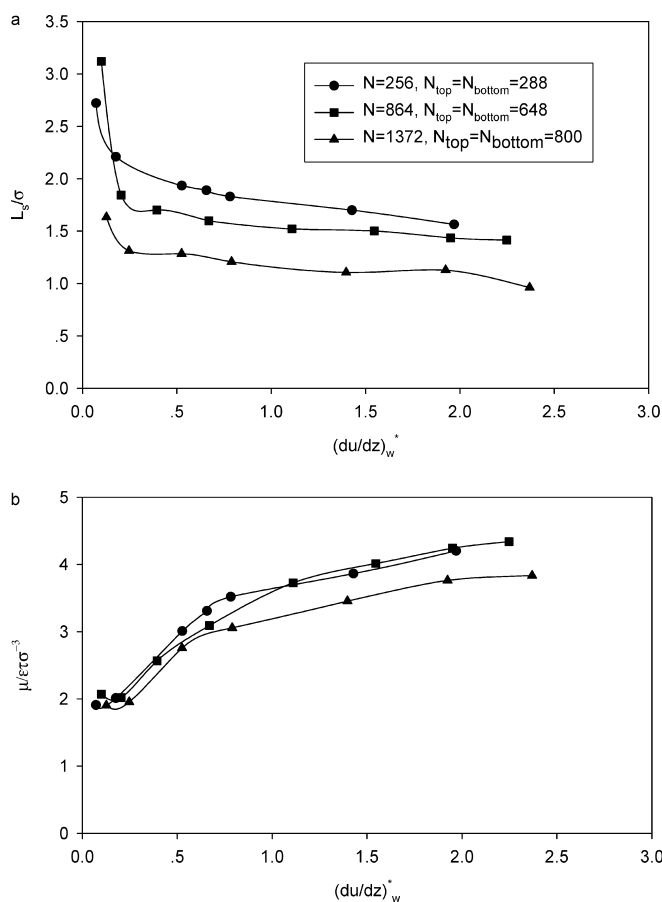


Fig. 10. Effect of shear rate on the slip length and viscosities at the wall surface

simulations require a lot of CPU time. The above analysis is consistent with that when a macroscale is reached, the no-slip solution is obtained.

The slip lengths versus the wall shear rate, as shown in Fig.10a, is very high at very small shear rate. This is because the mean axial velocity profile is much even at very small shear rate (gravity force), the liquid molecules at the wall surface should travel a long distance beyond the wall surface to reach the zero velocity as the wall surfaces. The

slip lengths are sharply decreased, then slightly decrease with increasing the wall shear rate (applied gravity force).

It is interesting to note the nondimensional viscosities against the wall shear rate, as shown in Fig. 10b. The nondimensional viscosities at the wall surface nearly remains a constant value of 2.0 when the nondimensional shear rate is less than around 0.25, leading to the Newtonian flow behavior. The nondimensional value of 2.0 is quite close to the previous MD studies with no-slip flow, providing the encouragement that our MD simulations are correct. However, the non-dimensional viscosities are increased with increasing the wall shear rate if the nondimensional shear rate is larger than around 0.25, leading to the non-Newtonian flow characteristics.

#### 4 Conclusions

The Poiseuille flow for liquid argon flowing in nanoscale channels formed by the two infinity walls are successfully modeled in the present paper. The nondimensional slip velocity, slip length and viscosity are used to characterize the distinct surface phenomena compared with the classical Poiseuille flow in macroscales. The following conclusions can be drawn as follows:

1. With varying the nondimensional applied gravity force, the flow behaves three distinct regions, the free molecular oscillation, coupling and the gravity force domain regions.
2. In the coupling region with the flow controlled by both the applied gravity force and the intermolecular force among particles, the nondimensional number density and the velocities are symmetric about the centerline of the channels, even though the number densities have larger oscillations near the wall. The velocities get the maximum value at the centerline of the channel.
3. For all the cases numerically tested, slip velocities occur at the wall surface. Such slip velocities are increased with increasing the wall shear rate produced by the applied gravity force. At a given wall shear rate, larger liquid argon system (larger channel size) results in smaller slip velocities.
4. At very small wall shear rate, the slip length is high. Such slip lengths are sharply decreased with increasing the wall shear rate, then slightly decrease with further increasing the wall shear rate.
5. The nondimensional viscosities remains nearly constant value of 2.0 in a narrow wall shear rate range below around 0.25, leading to the Newtonian flow behavior. The viscosities are increased with increasing the wall shear rate if the non-dimensional shear rate is larger than 0.25, leading to the non-Newtonian flow behavior.

#### References

1. Mohamed Gad-el-Hak (1999) The fluid mechanics of microdevices – the freeman scholar lecture. ASME J Fluids Eng 121(5): 5–33
2. Rostami AA; Mujumdar AS, Saniei AS (2002) Flow and heat transfer for gas flowing in microchannels: a review. Heat Mass Transfer 38: 359–367

3. Israelachvili JN (1986) Measurement of the viscosity of liquids in very thin films. *J Colloid Interface Sci* 110(1): 263–271
4. Gee ML; McGuiggan PM; Israelachvili JN; Homola AM (1990) Liquid to solidlike transitions of molecularly thin films under shear. *J Chem Phys* 93(3): 1895–1906
5. Chan DYC; Horn RG (1985) Drainage of thin liquid films. *J Chem Phys* 83(10): 5311–5324
6. Debye P; Cleland RL (1959) Flow of liquid hydrocarbons in porous vycor. *J Appl Phys* 30(6): 843–849
7. Maynes D; Webb AR (2002) Velocity profile characterization in sub-millimeter diameter tubes using molecular tagging velocimetry. *Exp Fluids* 32: 3–15
8. Koppik J; Banavar JR, Willemsen JF (1989) Molecular dynamics of fluid at solid surfaces. *Phys Fluids A* 1(5): 781–794
9. Liem SY; Brown D; Clarke JHR (1992) Investigation of the homogeneous-shear nonequilibrium-molecular-dynamics method. *Phys Rev A* 45(6): 3706–3713
10. Thompson PA; Robbins MO (1990) Shear flow near solids: Epitaxial order and flow boundary conditions. *Phys Rev A* 41(12): 6830–6837
11. Thompson PA; Troian SM (1997) A general boundary condition for liquid flow at solid surfaces. *Lett Nat* 389(25): 360–362
12. Yi P; Poulidakos D; Walther J; Yadigaroglu G (2002) Molecular dynamics simulation of vaporization of an ultra-thin liquid argon layer on a surface. *Int J Heat Mass Transfer* 45: 2087–2100
13. Haile JM (1992) *Molecular dynamics simulation*, Interscience, New York
14. Alexander FJ; Garcia AL (1997) The direct simulation monte-carlo method. *Comput Simulations* 11(6): 588–593
15. Tenenbaum A; Ciccotti G; Gallico R (1982) Stationary nonequilibrium states by molecular dynamics – Fourier’s law. *Phys Rev A* 25(5): 2778–2787